Influence of Shape and Gradient Refractive Index in the Accommodative Changes of Spherical Aberration in Nonhuman Primate Crystalline Lenses

Alberto de Castro,[1] Judith Birkenfeld,[1] Bianca Maceo,[2,3] Fabrice Manns,[2,3] Esdras Arrieta,[2] Jean-Marie Parel,[2–4] and Susana Marcos[1]

[1]Instituto de Óptica "Daza de Valdés," Consejo Superior de Investigaciones Científicas (CSIC), Madrid, Spain
[2]Ophthalmic and Biophysics Center, Bascom Palmer Eye Institute, University of Miami, Miller School of Medicine, Miami, Florida
[3]Biomedical Optics Laboratory, Department of Biomedical Engineering, University of Miami College of Engineering, Coral Gables, Florida
[4]Brien Holden Vision Institute, University of New South Wales, Sydney, Australia

Correspondence: Susana Marcos, Serrano, 121, 28006, Madrid, Spain; susana@io.cfmac.csic.es.

Submitted: March 8, 2013
Accepted: July 17, 2013

Citation: de Castro A, Birkenfeld J, Maceo B, et al. Influence of shape and gradient refractive index in the accommodative changes of spherical aberration in nonhuman primate crystalline lenses. *Invest Ophthalmol Vis Sci*. 2013;54:6197–6207. DOI: 10.1167/iovs.13-11996

Purpose. To estimate changes in surface shape and gradient refractive index (GRIN) profile in primate lenses as a function of accommodation. To quantify the contribution of surface shape and GRIN to spherical aberration changes with accommodation.

Methods. Crystalline lenses from 15 cynomolgus monkeys were studied in vitro under different levels of accommodation produced by a stretching system. Lens shape was obtained from optical coherence tomography (OCT) cross-sectional images. The GRIN was reconstructed with a search algorithm using the optical path measured from OCT images and the measured back focal length. The spherical aberration of the lens was estimated as a function of accommodation using the reconstructed GRIN and a homogeneous refractive index.

Results. The lens anterior and posterior radii of curvature decreased with increasing lens power. Both surfaces exhibited negative asphericities in the unaccommodated state. The anterior surface conic constant shifted toward less negative values with accommodation, while the value of the posterior remained constant. GRIN parameters remained constant with accommodation. The lens spherical aberration with GRIN distribution was negative and higher in magnitude than that with a homogeneous equivalent refractive index (by 29% and 53% in the unaccommodated and fully accommodated states, respectively). Spherical aberration with the equivalent refractive index shifted with accommodation toward negative values (−0.070 μm/diopter [D]), but the reconstructed GRIN shifted it farther (−0.124 μm/D).

Conclusions. When compared with the lens with the homogeneous equivalent refractive index, the reconstructed GRIN lens has more negative spherical aberration and a larger shift toward more negative values with accommodation.

Keywords: crystalline lens, gradient refractive index, spherical aberration, accommodation, GRIN

The aberrations of the eye are known to change with accommodation,[1–5] and these changes are related to modifications of the shape and internal structure of the crystalline lens. Several studies have reported the shape of the surfaces and the optics of the accommodating crystalline lens.[6–8] However, although of critical importance to understand the optical changes of the lens with accommodation, the relative contribution of the crystalline lens shape and GRIN to the change in the optical properties that the lens undergoes with accommodation is not known.

In the last few years, there have been increasing efforts to develop, quantify, and validate techniques to measure the shape of the crystalline lens. Phakometric techniques such as Purkinje,[9,10] Scheimpflug,[8,11,12] and more recently magnetic resonance imaging (MRI)[13,14] and optical coherence tomography (OCT),[15,16] have allowed the characterization of the crystalline lens in the unaccommodated state and as a function of accommodation.

The changes in the external geometry of the crystalline lens affect the distribution of the GRIN inside the lens. Different nondestructive methods have been proposed to estimate the lens GRIN distribution in vitro, including integral inversion methods,[17–21] optimization methods,[9,22–25] or densitometry-based methods.[14,26,27] A recent optimization technique using optical path differences measured with an OCT as input data[28,29] has shown similar reconstruction accuracy to ray tracing optimization-based techniques.[30] The OCT high resolution and data acquisition speed makes it very suitable to investigate the changes of the GRIN with accommodation. OCT also allows reliable measurements of the crystalline lens surface shapes, both in vivo and in vitro.[15,16]

Several studies reveal changes of the GRIN in human crystalline lenses with age, with a progressive flattening of the GRIN profile in older lenses,[14,25,26,29] likely associated to age-related changes of the lens spherical aberration with age. We have recently shown that the presence of the GRIN plays a critical role in the negative spherical aberration of the isolated porcine,[28,31] monkey (Maceo BM, et al. *IOVS* 2013;54:ARVO E-Abstract 4272), and human (Birkenfeld J, et al. *IOVS* 2013;54:ARVO E-Abstract 4267) in vitro lenses, and in its shift toward less negative values with age. Observations of the shift of spherical aberration in isolated porcine lens from negative values in virgin lenses to positive values after lens refilling with a homogeneous refractive index polymer also point to a fundamental role of the GRIN in the crystalline lens optical properties.[32]

Although there is increasing experimental evidence of GRIN distribution in the crystalline lens of several species, the redistribution of the GRIN in the accommodating lens has remained relatively unexplored. Garner and Smith[9] used Purkinje-based phakometry data in combination with a one-variable bielliptical GRIN model to predict the change of the lens focal length with accommodation. A more recent study attempted to use MRI in vivo[26] to study the changes in axial and equatorial GRIN profile modeled by power functions. Recent studies have investigated the lens power change with accommodation, and the role of the GRIN in cynomolgus monkeys and hamadryas baboons, assuming a value for the outer cortex refractive index.[33,34] The relative contribution of the GRIN to lens power appears to remain constant with accommodation.[9,34,35] This suggests that a homogenous index material in lens refilling procedure would be equally efficient in producing a refractive power change (assuming identical lens shape changes) than the natural lens GRIN material. However, the impact of the GRIN in the lens high order aberrations and their change with accommodation has never been studied experimentally.

Prior theoretical studies on the potential impact of the GRIN on accommodation point to an important contribution of the GRIN in the value[36,37] and change of spherical aberration with accommodation.[38] The GRIN, assumed to be adapted to the surface geometry, would therefore enhance the role of the change of the surface conic constants with accommodation.[39]

While the change in the geometrical shape of the lens and GRIN profile has been scarcely studied, there are numerous reports on the change in optical quality (and optical aberrations) of the eye with accommodation in vivo in humans[1–5,40] and nonhuman primates.[41,42] It is widely accepted that spherical aberration changes systematically toward more negative values with accommodation. These optical changes should be the result of geometrical and structural changes of the crystalline lens with accommodation. Changes in lens shape with accommodation were studied in vitro, using stretching devices to mimic the radial accommodative forces, both in human[43–45] and nonhuman primates.[34,46] The shift of spherical aberration with accommodation toward more negative values has also been reported in stretching experiments of in vitro human[43] and macaque monkey lenses (Maceo BM, et al. *IOVS* 2013;54:ARVO E-Abstract 4272; and Ref. 46). Although stretching does not reproduce all aspects of natural accommodation due to, among others, the absence of vitreous and intraocular pressure and differences in the direction of the forces involved in accommodation,[46] the good correspondence between the geometrical and optical changes in the lens as a function of accommodation measured in vivo and in vitro demonstrates that stretching is a good model.[41,43]

Nonhuman primates have been used in the literature as a model for myopia, emmetropization, or accommodation.[33,34,47,48] Both rhesus and cynomolgus monkeys are used as an experimental model to test emerging solutions for presbyopia correction.[49–51] Although there may be some differences in the growth of human and monkey lenses, the monkey's accommodation apparatus has been shown to be close to human (Augusteyn RC, et al. *IOVS* 2011;52:ARVO E-Abstract 1541), and to change in a similar way with age as the accommodation apparatus of a human does.[33,52,53] A full characterization of the cynomolgus monkey lens as a function of accommodation is therefore important to fully establish this species as a model for accommodation and presbyopia studies.

In this study, we present for the first time experimental measurements of the lens geometry (radius of curvature and asphericity) and of the reconstructed GRIN profiles (nucleus and surface refractive index and power exponents) as a function of accommodation. The contribution to the spherical aberration and its change with accommodation is calculated by means of ray tracing through a lens model using the experimentally measured external geometry and GRIN. The experiments were performed on cynomolgus monkey crystalline lenses in vitro, and accommodation was mimicked experimentally using a computer-controlled motorized stretcher.

Methods

Donor Tissue

We studied 15 young cynomolgus lenses (*Macaca fascicularis*) aged between 3.0 and 7.3 years (average 5.7 ± 1.1 years). All experiments adhered to the Association for Research in Vision and Ophthalmology Statement for the Use of Animals in Ophthalmic and Visual Research. The eyes were obtained from the Division of Veterinary Resources at the University of Miami as part of a tissue-sharing protocol and were used in accordance with Institutional Animal Care and Use Guidelines. The eyes were enucleated immediately after euthanasia, wrapped in gauze, and placed in a closed container. No animals were euthanized for the sole purpose of this study. Upon arrival at the laboratory, all eyes were either directly prepared for stretching experiments or refrigerated at 4°C before testing.[54] The time between euthanasia and use was 11 ± 14 (range, 1–48) hours in this study.

Tissue Preparation

The tissue preparation protocol has been described previously.[44,55] In summary, the sclera was bonded on the eight segments of the stretching device using cyanoacrylate. The segments fit 1 mm posterior to the limbus to the equator of the eye. The posterior calotte of the eye was dissected and posterior vitreous was carefully removed to leave the anterior vitreous and hyaloid membrane and ciliary body untouched. The tissue section was then transferred on a Petri dish placed on a retro-illuminated station positioned under the operation microscope, the cornea was dissected at the level of the limbus, meridional incisions were made in the sclera between the mobile segment to produce eight independent segments, and the iris was removed. The tissue section was then transferred to an ex vivo accommodation simulator (EVAS II, a stretcher designed in the Ophthalmic and Biomedical Center in the University of Miami [Miami, FL]).[55] During the dissection and the EVAS II testing experiment, the tissue was immersed in a chamber filled with Dulbecco's modified Eagle's medium (DMEM).[56]

Investigative Ophthalmology & Visual Science

Stretching

The EVAS II reproduces disaccommodation by simultaneous radial stretching of the eight scleral segments up to 2.5 mm. For this study, steps of 0.25 mm, resulting in 11 accommodative steps, were used except for two of the lenses where only six accommodative steps were measured.

OCT Imaging

Cross-sectional images of the crystalline lens were obtained with a custom designed time-domain OCT system that uses a superluminescent diode with a nearly Gaussian spectrum, a specified central wavelength of 825 nm, and a bandwidth of 25 nm. The system has an optical scan depth of 10 mm and an axial resolution of 12 μm in air (16 μm in the preservation medium). Images were recorded with 5000 points/A-line, 500 A-lines/B-scan, and a lateral scan length of 10 mm.[57]

Lens Back Vertex Power Measurements

The lens back vertex power was measured, for each stretching step, using a method previously described.[34,53] Essentially, the OCT light source was used to project a collimated circular ring with a 1.5-mm radius onto the center of the lens. Below the cuvette holding the lens and preservation medium, a charge-coupled device camera mounted on a vertical translation stage (GP-CX261; Panasonic, Osaka, Japan) was used to locate the focus. The mean position resulting from three stretching runs was used in a paraxial optical model to calculate the back vertex power of the lens in diopters (D). The accuracy of the measurements was determined to be ±0.5 D by calibration tests using a set of glass lenses.

Experimental Protocols

To obtain lens shape and avoid the optical distortions, testing was first performed with the lens anterior surface facing the OCT (anterior up, Fig. 1A) and then the segment was inverted with the posterior surface facing the OCT (posterior up, Fig. 1B). Following the stretching runs to image the lens, more stretching experiments were performed to measure the back vertex power of the lenses both anterior-up and posterior-up.

In all the measurements, the lenses were centered using the OCT system such that the specular reflection produced by the lens apex[57] was seen from the anterior or posterior surfaces of the lens. By placing the segments on an EVAS II in the same orientation for both anterior and posterior surfaces up, the same cross-section of the lens was analyzed.

OCT Image Analysis

The shape of the lens surfaces was obtained for each stretching position from the OCT images. The distortion of the first surface (anterior in anterior-up images and posterior in posterior-up images) is only due to the presence of DMEM; therefore, its correct shape can be extracted by dividing its height by the DMEM group refractive index. The segmented edges were fitted to conic sections.[58] The distorted surfaces (posterior in anterior-up image, anterior in posterior-up image, and cuvette in both) were detected and used as experimental input data to reconstruct the lens GRIN. In addition, the thickness of the lens and its average refractive index was calculated in both anterior-up and posterior-up images using the distorted image of the cuvette.[57] For all computations, the central 6-mm area of the lens was evaluated.

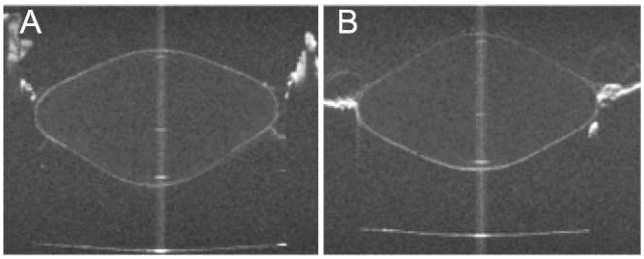

Figure 1. OCT images of the crystalline lens with the anterior surface facing the OCT beam (**A**) and with the posterior surface facing the OCT beam (**B**). The distorted surfaces contain the information of the optical path of the rays passing through the lens. These data, together with power measurements, are used in this study to reconstruct the gradient index of refraction of the lens. Images are for a 5.5-year-old cynomolgus lens fully accommodated.

GRIN Reconstruction

The OCT-based GRIN reconstruction technique has been described in detail in prior publications.[28,29] The height of the distorted surfaces in the OCT image is a recording of the optical path traveled by the light. A search algorithm was used to calculate the GRIN distribution that best matched the optical path accumulated by the rays passing through the lens and the back focal length measured. A 3-variable power equation model, described in detail in a previous study,[29] was used to model the GRIN. The model is described in polar coordinates with the origin on the optical axis at 0.41 times the central thickness of the lens, and is expressed by the following equation:

$$n(\rho,\theta) = n_N - (n_N - n_S) \times \left(\frac{\rho}{\rho(S,\theta)}\right)^p \qquad (1)$$

The parameters of this model are the nucleus (n_N) and surface (n_S) refractive indices (which are assumed constant across accommodation levels) and a power coefficient (p) (which varied across accommodation levels) to model the decay from nucleus to surface in all directions. The value $\rho(S, \theta)$ is the distance from the center to the conic surface in the direction θ. A ray trace using the Sharma algorithm[59] was programmed using numerical computation software (MATLAB; MathWorks, Natick, MA) to compute the optical path of the rays, and the results were compared with the experimental data. Input experimental data (optical path differences from OCT and lens power) collected for all stretching levels were pooled, and the optimization was performed simultaneously. The search algorithm was a mixture of a global (genetic algorithm of 20 generations of 200 solutions each) and a local search (simplex).[28] The reconstruction of the GRIN was achieved in 30 minutes, for a full series of lens data in 11 different stretching positions. The mean value of 10 repetitions of the search algorithm was taken as solution. Since the experimental data are obtained with the OCT light source, the measured GRIN values correspond with the group refractive indices at the OCT central wavelength (825 nm) and can be transformed to phase refractive indices at any wavelength.[57] The transformation is explained in detail in a previous publication.[57] In brief, the dispersion data from the literature[60] were used to transform the group refractive index to phase refractive index at 850 nm. The phase refractive index at any other wavelength can be calculated with the constant scaling formula derived by Atchison and Smith.[60]

Investigative Ophthalmology & Visual Science

Estimated Thickness of Lens Nucleus and Cortex

To study the contribution of the nucleus and the cortex to the change of lens thickness with accommodation, the nucleus was defined as the central lens region of the reconstructed GRIN for which the refractive index varies within 1% of the peak refractive index, following the definition proposed in previous studies.[26]

Estimated Power and Spherical Aberration

Virtual ray tracing was performed on the reconstructed lens (lens shape and GRIN) for a 6-mm pupil diameter (101 rays, ray spacing 30 μm), using the ray trace program written in MATLAB (MathWorks). Since the back vertex power was experimentally measured using the OCT beam, the group refractive index was used in the calculations. The back focal length was calculated as the distance from the posterior vertex of the lens to the position where the root mean squares of the ray heights reached a minimum. The estimated back focal length, calculated with the reconstructed GRIN, was used to estimate the equivalent refractive index, defined as the index of a lens with the same geometry and power as the crystalline lens. The error in the approximation of using the back vertex power instead of the power in the calculation of the equivalent refractive index was estimated for the mean geometry of the cynomolgus lenses. The wavefront was computed after the lens (assuming the exit pupil plane at the position of the lens posterior surface vertex). The wave aberration was estimated with respect to a reference sphere centered at the paraxial focal point. Wave aberration was fitted by a sixth order Zernike polynomial expansion. The fourth order spherical aberration Zernike coefficient was evaluated. Calculations were performed for both a homogeneous refractive index (equivalent index) and for the estimated GRIN profile. By definition, the lens power for the homogeneous equivalent refractive index and for the GRIN is the same. The spherical aberration, assuming a homogeneous refractive index or the GRIN, was evaluated in all accommodative steps. Also, the contributions of the lens surface geometry to lens power and to spherical aberration were calculated replacing the GRIN by a homogeneous refractive index equal to that of the surface (i.e., these were not calculated for each surface separately).

Results

Stretching Versus Refractive Change

Figure 2 shows the back vertex power decrease with stretching in all lenses. On average across lenses, back vertex power changed from 56 ± 4 D for 0-mm stretching to 29 ± 4 D at 2.5-mm stretching. In what follows, data will be plotted as a function of the measured lens back vertex power (corresponding to each of the stretching levels).

Changes of the Lens Geometry With Accommodation

The central 6 mm of the lens surfaces were well fitted to by conic sections.[58] The root mean square of the residuals of the fittings were below 20 μm in all the surfaces. The anterior and posterior radii of curvature decreased with accommodation (Figs. 3A, 3B). Changes with accommodation were larger in the anterior surface than in the posterior surface. The average unaccommodated anterior and posterior lens radii of curvature were 8.7 ± 1.2 and 4.5 ± 0.4 mm, respectively. Anterior lens radius decreased at a rate of 0.19 ± 0.04 mm/D, and the posterior lens radius at a rate of 0.067 ± 0.012 mm/D. The conic constant of the anterior surface showed large variability (not correlated with age or postmortem time), but was negative for all the lenses (with values from −14 to −2 in the unaccommodated state) and shifted toward less negative values with accommodation (Fig. 3C). The conic constant of the posterior surface remained near 0, and was rather constant in the entire accommodative range (Fig. 3D). Thickness increased linearly with accommodation at a rate of 0.036 ± 0.004 mm/D (Fig. 3E). All parameters varied almost linearly when plotted as a function of the back focal length. Except for anterior conic constant, all parameters varied similarly in all lenses.

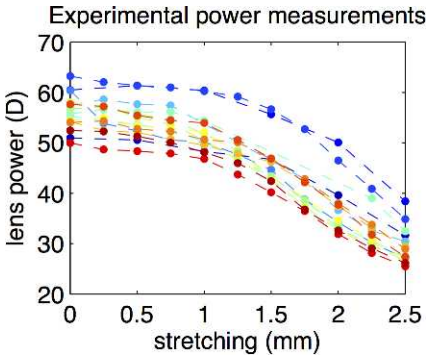

Figure 2. Back vertex power of all the studied lenses measured experimentally, as a function of stretching.

Changes of the Lens GRIN With Accommodation

Figure 4 shows the GRIN parameters from the reconstructed GRIN distributions in all lenses: surface and nucleus refractive indices (Fig. 4A) and the power exponent (Fig. 4B). The surface and nucleus refractive indices were 1.375 ± 0.003 and 1.429 ± 0.003, respectively, on average across lenses. The power exponent ranged from 2.1 to 9.1 across lenses. On average, the power exponent remained rather constant with accommodation showing a slight but nonsignificant ($P > 0.5$) increase with accommodation (average across lenses $p = 4.45 + 0.001 \times$ back vertex power [D]). The intersubject variability observed in the exponent was not correlated with age or postmortem time. The mean average values of surface and nucleus phase refractive indices at 633 nm were 1.365 and 1.419, respectively.

Figure 5A shows the lens average refractive index calculated directly from the OCT images. This parameter remains constant with accommodation. The equivalent refractive index (Fig. 5B) is also constant with accommodation, indicating that a similar power change would be achieved if the GRIN was replaced by the equivalent refractive index.

The equivalent refractive index was calculated using the back focal length. Simulations in an optical design program (Zemax; Radiant Zemax, Redmond, WA) show that differences in the estimated equivalent refractive index using focal length (measured from the principal plane) or back focal length differed less than 1% in both accommodated and unaccommodated states.

Contributions of Nucleus and Cortex to Lens Thickness

Figure 6A shows the thickness of the crystalline lens, nucleus, and cortex (as defined in the "Methods" section). Due to the constancy of the power exponent through

Investigative Ophthalmology & Visual Science

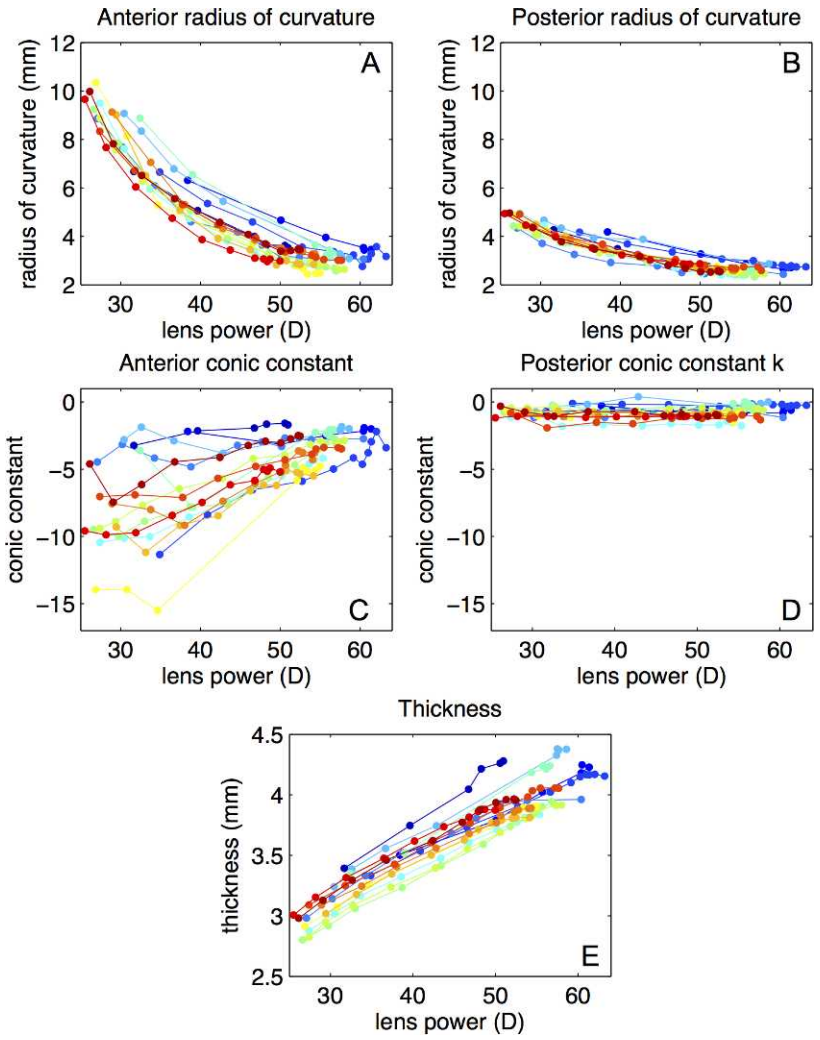

Figure 3. Lens geometry as a function of accommodation (stretching-induced changes in lens back vertex power). Using anterior-up and posterior-up images, the surface of the lens can be measured without optical distortion. (**A**) Anterior lens radius of curvature. (**B**) Posterior lens radius of curvature. (**C**) Anterior lens conic constant. (**D**) Posterior lens conic constant. (**E**) Lens thickness.

accommodation (Fig. 4B), the nucleus thickness accounted for a rather constant fraction of lens thickness (average value 73%). The change in lens thickness (0.035 mm/D) is mostly due to an increase in the nucleus thickness (0.024 mm/D) while the contribution to the change of thickness of the cortex is moderate (0.005 and 0.007 mm/D for the anterior and posterior cortex, respectively) with accommodation (Fig. 6B). During accommodation, the lens increases its thickness by a factor of 1.42. Relatively, the larger thickness change occurs at the cortex. The nucleus, anterior cortex, and posterior cortex sections increase by a factor of 1.38, 1.53, and 1.52, respectively).

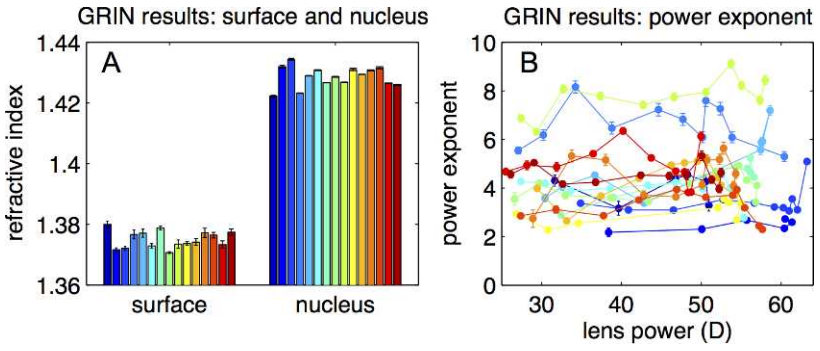

Figure 4. Results of the GRIN reconstruction. (**A**) Surface and nucleus refractive index. (**B**) Power exponent as a function of lens back vertex power.

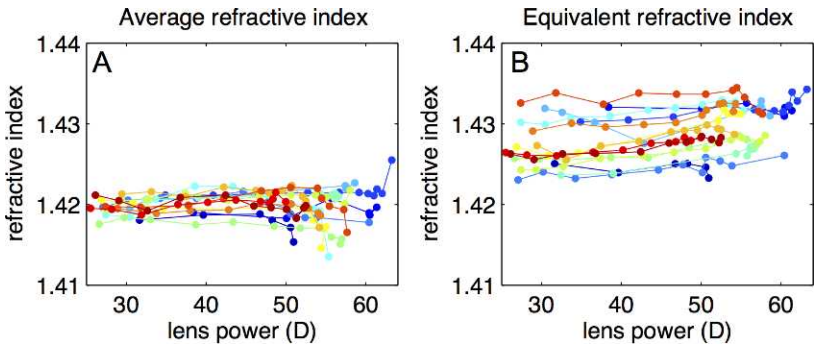

FIGURE 5. Average and equivalent refractive index. (**A**) Average refractive index estimated from the distortion present in the cuvette in the OCT images as a function of back vertex power. (**B**) Equivalent refractive index calculated from the back focal length for each accommodative state as a function of the back vertex power. The first index relates with the GRIN profile in optical axis and the second with the focal power of the crystalline lens (surface and GRIN).

Contributions to Lens Power Changes With Accommodation

The lens surface shape contributed on average 35% to 40% to the back vertex power of the crystalline lens in all accommodative states. The fact that this contribution is constant with accommodation indicates that the contribution of the external geometry to the amplitude of accommodation is similar. Surfaces contributed 8.4 ± 1.2 D to the amplitude of accommodation of the lens (27 ± 4 D), while GRIN was found responsible for almost 20 D of accommodation.

Spherical Aberration

The estimated spherical aberration was negative throughout the accommodative range, with values of −2.3 ± 0.7 μm for the unaccommodated state and −5.6 ± 1.5 μm in the fully accommodated state. Figure 7 shows a comparison between the spherical aberration of the lens with the estimated GRIN and with the equivalent refractive index, assuming the measured lens geometry in both cases. The intersubject variability was not correlated with age or postmortem time The spherical aberration magnitude assuming the equivalent index is lower compared with that found in the GRIN lens, with a larger difference in the fully accommodated state (53% on average) than in the unaccommodated state (29% on average). The spherical aberration increased in absolute value with accommodation at a rate of 0.124 μm/D on average (for the lens with the calculated GRIN) and at a rate of 0.070 μm/D on average (for the lens with the equivalent refractive index).

Spherical Aberration Changes With Accommodation: Contribution of the Surfaces

The spherical aberration of a homogeneous lens with an index equal to the surface refractive index (Fig. 8A) varied between −0.25 ± 0.06 and −1.2 ± 0.3 μm. The relative contribution of the surfaces' spherical aberration to the total spherical aberration of the lens was 19% on average (Fig. 8B). This contribution increased slightly from the unaccommodated state (12 ± 4%) to the fully accommodated crystalline lens (21 ± 6%). Figure 8C shows the change of the spherical aberration with the calculated GRIN, 3.8 ± 1.2 μm as an average, and with homogeneous lens with index equal to the surface refractive index, 0.9 ± 0.2 μm. Figure 8D shows the contribution of GRIN and surfaces to the change of spherical aberration. On average, the gradient refractive index was found to be responsible for 73 ± 9% of the spherical aberration change of the lens.

Discussion

During accommodation, the primate crystalline lens changes its shape and the gradient index of refraction redistributes, producing well-known changes in the optical properties of the

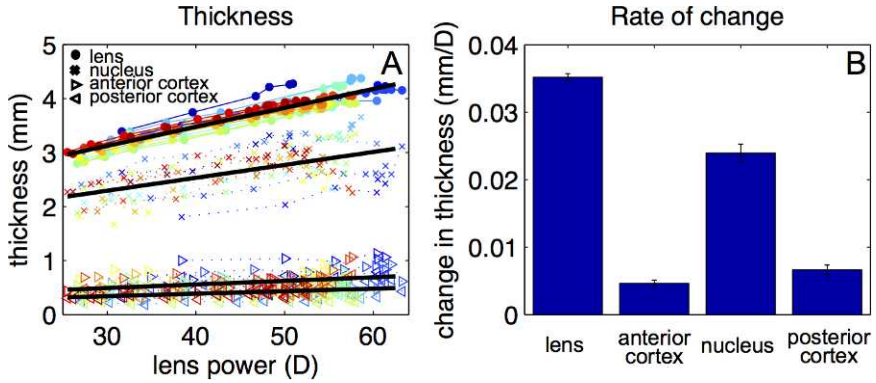

FIGURE 6. Thickness change with accommodation. (**A**) Thickness of the crystalline lens, nucleus, and the anterior and posterior cortex as a function of back vertex power for all lenses. *Black lines* represent linear fits to the data: total thickness (mm) = 2.070 + 0.035 × lens power (D); nucleus thickness (mm) = 1.576 + 0.0239 × lens power (D); anterior cortex thickness = 0.202 + 0.005 × lens power (D); and posterior cortex thickness = 0.291 + 0.007 × lens power (D). (**B**) Rate of change of the thickness of the lens, anterior cortex, nucleus, and posterior cortex of the lens.

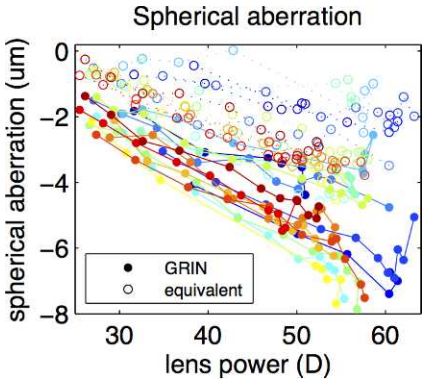

Figure 7. Spherical aberration as a function of lens back vertex power through accommodation, for the lens with the reconstructed GRIN (*solid circles*) and with the equivalent refractive index (*empty circles*).

crystalline lens: an increase of power and a shift of the spherical aberration toward more negative values. We have presented experimental measurements of the changes of both the geometry of the crystalline lens, and of the GRIN profile of nonhuman primate lenses (cynomolgus monkeys) with accommodation. Accommodation was simulated in vitro using a stretching device, a paradigm that has been previously demonstrated to mimic accurately the change in lens shape and power occurring in vivo.[41,43,45,53] These measurements have allowed us to quantify the role of the GRIN in accommodation, and to estimate the relative contribution of surface and GRIN to lens power—and most notably, to the spherical aberration, as a function of accommodation. All the results presented in this study were calculated using the group refractive index at 825 nm in both the crystalline lens and the preservation medium (DMEM, 1.345). To check the validity of the results in visible light, the ray tracing was repeated with the surface and nucleus refractive index converted to phase refractive index at 555 nm and assuming an aqueous and vitreous refractive index of 1.336. The differences between group refractive index and phase refractive index are around 1% (0.007 as a mean), producing average differences in power and spherical aberration below 3% (1.1 D and below 0.1 μm, respectively).

In agreement with previously reported in vivo and in vitro data in humans[8,9] and in rhesus monkey lenses,[11,61] we found a decrease in the lens surface radii of curvature with accommodation, larger for the anterior surface than for the posterior surface. The slightly smaller change per diopter of accommodation in cynomolgus monkeys may be due to interspecies differences, age differences, and the high asphericity of the anterior surface.

Very few studies have reported crystalline lens asphericity. We found that the anterior surface conic constant of the unaccommodated cynomolgus lens was consistently negative (although it varied significantly across individuals, ranging from −14 to −2) and decreased in most of the lenses toward a more spherical shape with accommodation. The posterior conic constant was also negative but close to zero and remained constant with accommodation. These data differ from reports in human lenses in vivo,[8] measured with Scheimpflug imaging, where both anterior and posterior surfaces had negative asphericity with similar mean values, although the intersubject variability was very large. Also, the change with accommodation differs, as in humans the anterior surface seems to become more curved with the peripheral areas of the lens remaining relatively flatter, and therefore the conic constant changes toward more negative values. However, the results in human lenses in vivo[8] show small changes in the anterior conic constant with accommodation, and no accommodation-related changes in the posterior surface conic constant due to limitations in the technique. Studies in in vitro–human crystalline lenses[58] reported a positive conic constant in the

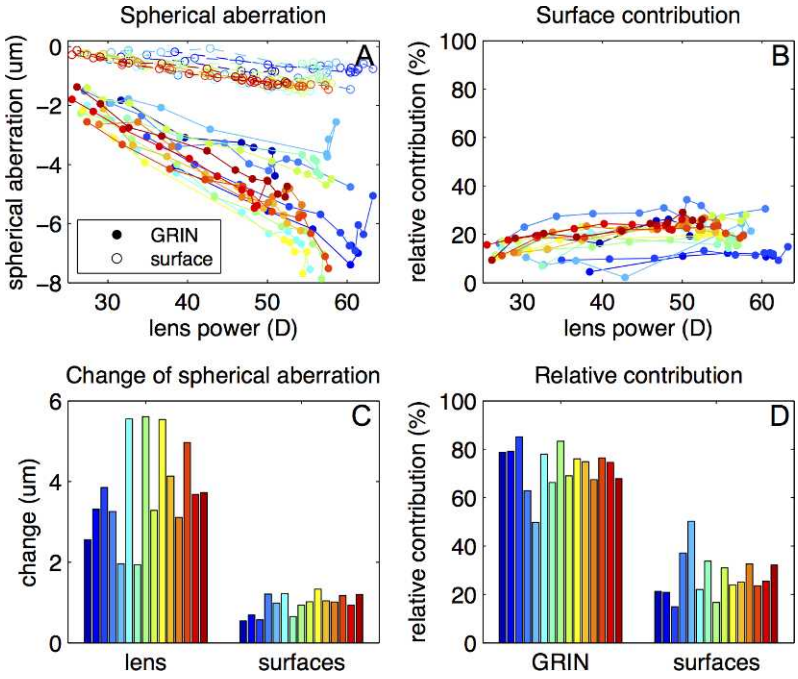

Figure 8. Contribution of the surfaces to the spherical aberration. (**A**) Spherical aberration of the lens with GRIN compared with that of a homogeneous lens with index equal to the surface refractive index as a function of back vertex power. (**B**) Contribution of the surface to the magnitude of Spherical aberration as a function of back vertex power. (**C**) Change in absolute value of spherical aberration of the lens compared with that of the surfaces from unaccommodated to fully accommodated. (**D**) Relative contribution of the surface and GRIN to the change of spherical aberration with accommodation.

anterior surface and scattered values of approximately 0 for the posterior. The values of asphericity reported here for the fully accommodated state agrees well with those reported by a previous study in isolated cynomolgus monkey lenses,[33] where a wide range (from –6 to +4) was reported. The high value of lens anterior surface asphericity in monkeys in the unaccommodated state, never reported in humans, may be due to the differences in size between the species, to the young age of the monkey lenses compared with the humans from prior literature, and to the larger accommodative range of monkey lenses (up to 30 D) in comparison with the human lens (no more than 10 D).

We found that the lens thickness increased with accommodation at a rate of 0.036 ± 0.004 mm/D. This thickness variation is comparable to that reported in vivo in rhesus monkeys under stimulated accommodation, around 0.041 mm/D[11] and 0.063 mm/D,[62] and in vivo in humans, 0.045 mm/D[8] and 0.064 mm/D.[63]

In agreement with previous findings, we have found that a rather constant value of the parameters defining the GRIN best fitted the experimental data[9,35] and that the equivalent refractive index did not change with accommodation.[9,34,35]

Despite the simplicity of the GRIN model, the estimated parameters allow reproducing the experimental input data with great accuracy (mean RMS < 40 μm), for all accommodation levels, using our recently developed optimization method based on OCT imaging.[28] Previous studies with simpler GRIN models suggested that no change in the parameters of the model was needed to account for a change of power of the crystalline lens with accommodation.[9,35] We have found a slight trend for an increase in the power exponent parameter of our GRIN model (expansion of the central plateau in the GRIN distribution), although this was not statistically significant. This was in contrast with a report using MRI,[26] which suggested a decrease of this parameter (only significant in the meridional direction), and a 50% contribution of the lens thickness nucleus to the change of lens thickness with accommodation. Studies based on Scheimpflug imaging revealed a much higher contribution of the lens nucleus (90%) in humans[6,64,65] and rhesus monkey.[66] While differences arising from the definition of the lens nucleus and the data analysis are expected, our study on cynomolgus monkeys also supports a large contribution of the lens nucleus in thickness changes (69%, following the definition proposed by Kasthurirangan et al.[26]). This conclusion is highly dependent of the adopted definition for the nucleus. While the current definition does not necessarily best describe the physiological area of the lens nucleus, it allows comparison with prior literature using this definition.[26] Nevertheless, the estimated nucleus thickness relative to the total thickness (73%) with that definition is only slightly larger than that obtained from direct imaging of the lens (65%, from Scheimpflug imaging in young human subjects in vivo[64]; 57% from OCT imaging as an average in isolated human crystalline lenses of different ages [de Freitas C, et al. *IOVS* 2013;52:ARVO E-Abstract 818]).

We found the spherical aberration of the unaccommodated cynomolgus lens to be negative (–2.3 μm, 6-mm pupil diameter), as reported in young human lenses (–0.16 μm, 6-mm pupil in vivo[67]) and rhesus monkey (–1 μm, 7-mm in vitro[46] and –0.5 μm, 8-mm in vivo[41]). Previous studies have reported a compensatory role of the GRIN in different species such as fish,[68] rat,[69] porcine lenses,[28,32,70] and also in humans (Birkenfeld J, et al. *IOVS* 2011;52:ARVO E-Abstract 3404). With those lens geometries, and with a homogeneous index of refraction, the spherical aberration of the lens was positive, and the presence of GRIN shifted the lens toward less positive values (or close to zero, such as in fish) or toward negative values, which tended to compensate the positive spherical aberration of the cornea. In cynomolgus lenses, we have also found a compensatory role of GRIN. However, in this case, the GRIN did not reverse the sign of the spherical aberration, already negative with an equivalent refractive index, but rather doubled its magnitude. The spherical aberration value of the lens with an equivalent refractive index was on average 41% of that of the corresponding GRIN lens. Also, the presence of GRIN emphasized the change of spherical aberration with accommodation. The change in spherical aberration with accommodation estimated with the equivalent refractive index was on average 29% of the change for the corresponding GRIN lens. While there is a large intersubject variability (which we did not find to be correlated with age or postmortem time), we have found that the contribution of GRIN in the spherical aberration is slightly larger in the fully accommodated state.

As in rhesus monkeys,[41,46] we found a shift of the spherical aberration during accommodation toward more negative values. We found larger differences (unaccommodated to fully accommodative state) in spherical aberration in cynomolgus (3.3 μm for a 6-mm pupil) than in rhesus monkeys (around 2 μm, 8-mm, in vivo[41]; 1.7 μm, 7-mm, in vitro[46]). However, as the accommodation amplitude is larger in cynomolgus (20–30 D) than in rhesus (around 17 D), the shift of spherical aberration per diopter of accommodation appears relatively similar across species (–0.124 μm/D in the current study in cynomolgus monkeys; around –0.11 μm/D in vitro[46] and –0.19 and –0.24 μm/D in vivo[41] in rhesus). These values are higher than those reported in humans for 6-mm (–0.013 μm/D[5], –0.083 μm/D[3]). The calculated spherical aberration value may be affected by errors in the calculation of the geometry of the surfaces of the crystalline lens, in the reconstruction of GRIN and in the accuracy of the GRIN model itself.

As in previous studies,[9,34,37,38,71] the contributions of the GRIN to the power and spherical aberration were computed by comparing the lens optical properties with those produced by refraction in the surfaces only. While previous publications assumed a fixed surface refractive index to estimate the contribution of the surfaces to the change of power of the lens, in this study the surface index was obtained directly for each lens from the GRIN reconstructed from the experimental data. The contribution of the GRIN to the power and accommodative amplitude of the lens reported is in agreement with previous studies in vitro in baboon and cynomolgus monkeys[34] and in humans.[34,53] For spherical aberration, we found that the surface contribution was around 20%, and that the contribution was larger in the fully accommodated state. These results are indicative of a large contribution (almost 80%) of the GRIN to the value of lens spherical aberration in the entire accommodative range. Also, the redistribution of the GRIN was found to be responsible for more than 70% of the change of spherical aberration through accommodation.

For these calculations, we defined the spherical aberration contribution of the GRIN as the difference between the spherical aberration of the reconstructed GRIN lens and the spherical aberration of a lens with a homogeneous refractive index equal to that of the surface, in a similar way as previously evaluated for the surface/GRIN contributions to the power of the lens.[9,34,53,71] There are other possible definitions or values of the index of the homogeneous lens that could be used, which may produce different numerical results, but we expect that the general finding regarding the importance of the GRIN will not change. For instance, our analysis shows that the change in spherical aberration of the lens with homogeneous index equal to the equivalent index

Investigative Ophthalmology & Visual Science

(instead of the surface index) is still only 56% of the change found with the GRIN lens.

Theoretical analyses[72,73] have shown that model eyes that simulate the change of spherical aberration with accommodation can be designed using a lens model with a shape, and a homogeneous equivalent refractive index ($n = 1.429$), based on the measurements of Dubbelman et al.[8] However, this lens model does not provide accurate predictions of the actual value of lens spherical aberration, most likely due to uncertainties in the lens surface asphericity values.[72] Our experimental study on monkey lenses is in disagreement with the conclusion of Lopez-Gil and Fernandez-Sanchez,[73] regarding the contribution of the GRIN to the change of spherical aberration with accommodation. We find that the equivalent homogeneous lens predicts the general trend of the change in spherical aberration with accommodation, but it does not reproduce the actual spherical aberration value and its change with accommodation, obtained with experimental measurements of the crystalline lens shape and GRIN.

The literature on the changes of the GRIN distribution with accommodation is scarce and to our knowledge, this is the first study that explores experimentally this redistribution in nonhuman primate lenses and studies its influence in the spherical aberration of the eye. This study has contributed to a deeper understanding of the role and relative importance of the gradient refractive index on the optics of the crystalline lens.

Acknowledgments

Supported by a Spanish government Grant FIS2011-25637 and the European Research Council ERC-AdG-294099 (SM); CSIC JAE-Pre Program fellowship (JB); CSIC i-LINK+ 2012, i-LINK+0609 (SM, J-MP); National Eye Institute Grants 2R01EY14225, 1R01EY021834, 1F31EY021444 (NSRA Individual Predoctoral Fellowship [BM]), P30EY14801 (Center Grant); the Florida Lions Eye Bank; the Henri and Flore Lesieur Foundation (J-MP); Research to Prevent Blindness; the Vision Cooperative Research Centre, Sydney, New South Wales, Australia; and the Australian Federal Government through the Cooperative Research Centres Programme.

Disclosure: **A. de Castro**, None; **J. Birkenfeld**, None; **B. Maceo**, None; **F. Manns**, None; **E. Arrieta**, None; **J.-M. Parel**, None; **S. Marcos**, None

References

1. Lu C, Munger R, Campbell MCW. Monochromatic aberrations in accommodated eyes. In: *Ophthalmic and Visual Optics. Noninvasive Assessment of the Visual System*. 1993 Technical Digest Series, vol. 3. Washington, DC: Optical Society of America; 1993:160–163.
2. Atchison DA, Collins MJ, Wildsoet CF, Christensen J, Waterworth MD. Measurement of monochromatic ocular aberrations of human eyes as a function of accommodation by the Howland aberroscope technique. *Vision Res*. 1995;35:313–323.
3. He JC, Burns SA, Marcos S. Monochromatic aberrations in the accommodated human eye. *Vision Res*. 2000;40:41–48.
4. Cheng H, Barnett JK, Vilupuru AS, et al. A population study on changes in wave aberrations with accommodation. *J Vis*. 2004;4:272–280.
5. Gambra E, Sawides L, Dorronsoro C, Marcos S. Accommodative lag and fluctuations when optical aberrations are manipulated. *Invest Ophthalmol Vis Sci*. 2009;9:4.1–4.15.
6. Brown N. The change in shape and internal form of the lens of the eye on accommodation. *Exp Eye Res*. 1973;15:441–459.
7. Koretz JF, Handelman GH, Brown NP. Analysis of human crystalline lens curvature as a function of accommodative state and age. *Vision Res*. 1984;24:1141–1151.
8. Dubbelman M, van der Heijde RGL, Weeber HA. Change in shape of the aging human crystalline lens with accommodation. *Vision Res*. 2005;45:117–132.
9. Garner LF, Smith G. Changes in equivalent and gradient refractive index of the crystalline lens with accommodation. *Optom Vis Sci*. 1997;74:114–119.
10. Rosales P, Marcos S. Phakometry and lens tilt and decentration using a custom-developed Purkinje imaging apparatus: validation and measurements. *J Opt Soc Am A Opt Image Sci Vis*. 2006;23:509–520.
11. Koretz JF, Bertasso AM, Neider MW, True-Gabelt BA, Kaufman PL. Slit-lamp studies of the rhesus monkey eye: II. Changes in crystalline lens shape, thickness and position during accommodation and aging. *Exp Eye Res*. 1987;45:317–326.
12. Dubbelman M, van der Heijde RGL. The shape of the aging human lens: curvature, equivalent refractive index and the lens paradox. *Vision Res*. 2001;41:1867–1877.
13. Strenk SA, Semmlow JL, Strenk LM, Munoz P, Gronlund-Jacob J, DeMarco JK. Age-related changes in human ciliary muscle and lens: a magnetic resonance imaging study. *Invest Ophthalmol Vis Sci*. 1999;40:1162–1169.
14. Moffat BA, Atchison DA, Pope JM. Age-related changes in refractive index distribution and power of the human lens as measured by magnetic resonance micro-imaging in vitro. *Vision Res*. 2002;42:1683–1693.
15. Borja D, Siedlecki D, de Castro A, et al. Distortions of the posterior surface in optical coherence tomography images of the isolated crystalline lens: effect of the lens index gradient. *Biomed Opt Express*. 2010;1:1331–1340.
16. Ortiz S, Pérez-Merino P, Gambra E, de Castro A, Marcos S. In vivo human crystalline lens topography. *Biomed Opt Express*. 2012;3:2471–2488.
17. Campbell MC. Measurement of refractive index in an intact crystalline lens. *Vision Res*. 1984;24:409–415.
18. Pierscionek BK. Growth and ageing effects on the refractive index in the equatorial plane of the bovine lens. *Vision Res*. 1989;29:1759–1766.
19. Pierscionek BK, Belaidi A, Bruun HH. Refractive index distribution in the porcine eye lens for 532 nm and 633 nm light. *Eye (Lond)*. 2005;19:375–381.
20. Acosta E, Vazquez D, Garner L, Smith G. Tomographic method for measurement of the gradient refractive index of the crystalline lens. I. The spherical fish lens. *J Opt Soc Am A*. 2005;22:424–433.
21. Vazquez D, Acosta E, Smith G, Garner L. Tomographic method for measurement of the gradient refractive index of the crystalline lens. II. The rotationally symmetrical lens. *J Opt Soc Am A*. 2006;23:2551–2565.
22. Axelrod D, Lerner D, Sands PJ. Refractive index within the lens of a goldfish eye determined from the paths of thin laser beams. *Vision Res*. 1988;28:57–65.
23. Garner LF, Smith G, Yao S, Augusteyn RC. Gradient refractive index of the crystalline lens of the Black Oreo Dory (Allocyttus Niger): comparison of magnetic resonance imaging (MRI) and laser ray-trace methods. *Vision Res*. 2001;41:973–979.
24. Pomerantzeff O, Fish H, Govignon J, Schepens CL. Wide-angle optical model of the eye. *J Mod Opt*. 1972;19:387–388.
25. Hemenger RP, Garner LF, Ooi CS. Change with age of the refractive index gradient of the human ocular lens. *Invest Ophthalmol Vis Sci*. 1995;36:703–707.
26. Kasthurirangan S, Markwell EL, Atchison DA, Pope JM. In vivo study of changes in refractive index distribution in the human crystalline lens with age and accommodation. *Invest Ophthalmol Vis Sci*. 2008;49:2531–2540.

27. Hoshino M, Uesugi K, Yagi N, Mohri S, Regini J, Pierscionek B. Optical properties of in situ eye lenses measured with X-ray Talbot interferometry: a novel measure of growth processes. *PLoS One*. 2011;6:e25140.
28. de Castro A, Ortiz S, Gambra E, Siedlecki D, Marcos S. Three-dimensional reconstruction of the crystalline lens gradient index distribution from OCT imaging. *Opt Express*. 2010;18: 21905–21917.
29. de Castro A, Siedlecki D, Borja D, et al. Age-dependent variation of the gradient index profile in human crystalline lenses. *J Mod Opt*. 2011;58:1781–1787.
30. de Castro A, Barbero S, Ortiz S, Marcos S. Accuracy of the reconstruction of the crystalline lens gradient index with optimization methods from ray tracing and Optical Coherence Tomography data. *Opt Express*. 2011;19:19265–19279.
31. Birkenfeld J, de Castro A, Ortiz S, et al. Contribution of the gradient refractive index and shape to the crystalline lens spherical aberration and astigmatism. *Vision Res*. 2013;86:27–34.
32. Wong K-H, Koopmans SA, Terwee T, Kooijman AC. Changes in spherical aberration after lens refilling with a silicone oil. *Invest Ophthalmol Vis Sci*. 2007;48:1261–1267.
33. Borja D, Manns F, Ho A, et al. Refractive power and biometric properties of the nonhuman primate isolated crystalline lens. *Invest Ophthalmol Vis Sci*. 2010;51:2118–2125.
34. Maceo BM, Manns F, Borja D, et al. Contribution of the crystalline lens gradient refractive index to the accommodation amplitude in non-human primates: In vitro studies. *J Vis*. 2011;11:23.
35. Hermans EA, Dubbelman M, van der Heijde RGL, Heethaar RM. Equivalent refractive index of the human lens upon accommodative response. *Optom Vis Sci*. 2008;85:1179–1184.
36. Díaz JA, Fernández-Dorado J, Sorroche F. Role of the human lens gradient-index profile in the compensation of third-order ocular aberrations. *J Biomed Opt*. 2012;17:075003.
37. Bahrami M, Goncharov AV. Geometry-invariant gradient refractive index lens: analytical ray tracing. *J Biomed Opt*. 2012;17:055001.
38. Smith G, Bedggood P, Ashman R, Daaboul M, Metha A. Exploring ocular aberrations with a schematic human eye model. *Opt Vis Sci*. 2008;85:330–340.
39. Navarro R, Palos F, González LM. Adaptive model of the gradient index of the human lens. II. Optics of the accommodating aging lens. *J Opt Soc Am A*. 2007;24:2911–2920.
40. Plainis S, Ginis HS, Pallikaris A. The effect of ocular aberrations on steady-state errors of accommodative response. *J Vis*. 2005; 5:466–477.
41. Vilupuru AS, Roorda A, Glasser A. Spatially variant changes in lens power during ocular accommodation in a rhesus monkey eye. *J Vis*. 2004;4:299–309.
42. Vilupuru AS, Kasthurirangan S, Glasser A. Dynamics of accommodative fatigue in rhesus monkeys and humans. *Vision Res*. 2005;45:181–191.
43. Glasser A, Campbell MC. Presbyopia and the optical changes in the human crystalline lens with age. *Vision Res*. 1998;38: 209–229.
44. Manns F, Parel JM, Denham D, et al. Optomechanical response of human and monkey lenses in a lens stretcher. *Invest Ophthalmol Vis Sci*. 2007;48:3260–3268.
45. Augusteyn RC, Mohamed A, Nankivil D, et al. Age-dependence of the optomechanical responses of ex vivo human lenses from India and the USA, and the force required to produce these in a lens stretcher: the similarity to in vivo disaccommodation. *Vision Res*. 2011;51:1667–1678.
46. Roorda A, Glasser A. Wave aberrations of the isolated crystalline lens. *J Vis*. 2004;4:250–261.
47. Croft MA, Kaufman PL, Crawford KS, Neider MW, Glasser A, Bito LZ. Accommodation dynamics in aging rhesus monkeys. *Am J Physiol*. 1998;275:R1885–R1897.
48. Wendt M, Croft MA, McDonald J, Kaufman PL, Glasser A. Lens diameter and thickness as a function of age and pharmacologically stimulated accommodation in rhesus monkeys. *Exp Eye Res*. 2008;86:746–752.
49. Haefliger E, Parel JM. Accommodation of an endocapsular silicone lens (Phaco-Ersatz) in the aging rhesus monkey. *J Refract Corneal Surg*. 1994;10:550–555.
50. Nishi O, Nishi K. Accommodation amplitude after lens refilling with injectable silicone by sealing the capsule with a plug in primates. *Arch Ophthalmol*. 1998;116:1358–1361.
51. Koopmans SA, Terwee T, Glasser A, et al. Accommodative lens refilling in rhesus monkeys. *Invest Ophthalmol Vis Sci*. 2006; 47:2976–2984.
52. Qiao-Grider Y, Hung L-F, Kee C-S, Ramamirtham R, Smith R, Earl L. Normal ocular development in young rhesus monkeys (Macaca mulatta). *Vision Res*. 2007;47:1424–1444.
53. Borja D, Manns F, Ho A, et al. Optical power of the isolated human crystalline lens. *Invest Ophthalmol Vis Sci*. 2008;49: 2541–2548.
54. Nankivil D, Manns F, Arrieta-Quintero E, et al. Effect of anterior zonule transection on the change in lens diameter and power in cynomolgus monkeys during simulated accommodation. *Invest Ophthalmol Vis Sci*. 2009;50:4017–4021.
55. Ehrmann K, Ho A, Parel J-M. Biomechanical analysis of the accommodative apparatus in primates. *Clin Exp Optom*. 2008; 91:302–312.
56. Augusteyn RC, Rosen AM, Borja D, Ziebarth NM, Parel JM. Biometry of primate lenses during immersion in preservation media. *Mol Vis*. 2006;12:740–747.
57. Uhlhorn SR, Borja D, Manns F, Parel JM. Refractive index measurement of the isolated crystalline lens using optical coherence tomography. *Vision Res*. 2008;48:2732–2738.
58. Manns F, Fernandez V, Zipper S, et al. Radius of curvature and asphericity of the anterior and posterior surface of human cadaver crystalline lenses. *Exp Eye Res*. 2004;78:39–51.
59. Sharma A, Kumar DV, Ghatak AK. Tracing rays through graded-index media: a new method. *Appl Opt*. 1982;21:984–987.
60. Atchison DA, Smith G. Chromatic dispersions of the ocular media of human eyes. *J Opt Soc Am A*. 2005;22:29–37.
61. Rosales P, Wendt M, Marcos S, Glasser A. Changes in crystalline lens radii of curvature and lens tilt and decentration during dynamic accommodation in rhesus monkeys. *J Vis*. 2008;8: 18.11–1812.
62. Vilupuru AS, Glasser A. The relationship between refractive and biometric changes during Edinger-Westphal stimulated accommodation in rhesus monkeys. *Exp Eye Res*. 2005;80: 349–360.
63. Richdale K, Sinnott LT, Bullimore MA, et al. Quantification of age-related and per diopter accommodative changes of the lens and ciliary muscle in the emmetropic human eye. *Invest Ophthalmol Vis Sci*. 2013;54:1095–1105.
64. Dubbelman M, van der Heijde RGL, Weeber HA, Vrensen GFJM. Changes in the internal structure of the human crystalline lens with age and accommodation. *Vision Res*. 2003;43:2363–2375.
65. Hermans EA, Dubbelman M, van der Heijde RGL, Heethaar R. The shape of the human lens nucleus with accommodation. *J Vis*. 2007;7:16.1–16.10.
66. Koretz JF, Bertasso AM, Neider MW, Kaufman PL. Slit-lamp studies of the rhesus monkey eye: III. The zones of discontinuity. *Exp Eye Res*. 1988;46:871–880.
67. Barbero S, Marcos S, Merayo-Lloves J. Corneal and total optical aberrations in a unilateral aphakic patient. *J Cataract Refract Surg*. 2002;28:1594–1600.

Investigative Ophthalmology & Visual Science

68. Jagger WS. The optics of the spherical fish lens. *Vision Res*. 1992;32:1271–1284.

69. Campbell MC, Hughes A. An analytic, gradient index schematic lens and eye for the rat which predicts aberrations for finite pupils. *Vision Res*. 1981;21:1129–1148.

70. Vázquez Martínez D. *Tomographic Reconstruction of the Gradient Indices with Rotational Symmetry. Application to Crystalline Lenses*. Santiago de Compostela: Universidad de Santiago de Compostela; 2007.

71. Jones CE, Atchison DA, Meder R, Pope JM. Refractive index distribution and optical properties of the isolated human lens measured using magnetic resonance imaging. *Vision Res*. 2005;45:2352–2366.

72. Norrby S. The Dubbelman eye model analysed by ray tracing through aspheric surfaces. *Ophthalmic Physiol Opt*. 2005;25: 153–161.

73. Lopez-Gil N, Fernandez-Sanchez V. The change of spherical aberration during accommodation and its effect on the accommodation response. *J Vis*. 2010;10:1–15.

Investigative Ophthalmology & Visual Science